

Wind profiles of tropical cyclones as observed by Doppler wind profiler and anemometer

Y.C. He¹, P.W. Chan² and Q.S. Li^{*1}

¹Department of Civil and Architectural Engineering, City University of Hong Kong, Hong Kong

²Hong Kong Observatory, Kowloon, Hong Kong

(Received April 8, 2011, Revised March 29, 2013, Accepted March 30, 2013)

Abstract. This paper investigates the vertical profiles of horizontal mean wind speed and direction based on the synchronized measurements from a Doppler radar profiler and an anemometer during 16 tropical cyclones at a coastal site in Hong Kong. The speed profiles with both open sea and hilly exposures were found to follow the log-law below a height of 500 m. Above this height, there was an additional wind speed shear in the profile for hilly upwind terrain. The fitting parameters with both the power-law and the log-law varied with wind strength. The direction profiles were also sensitive to local terrain setups and surrounding topographic features. For a uniform open sea terrain, wind direction veered logarithmically with height from the surface level up to the free atmospheric altitude of about 1200 m. The accumulated veering angle within the whole boundary layer was observed to be 30°. Mean wind direction under other terrain conditions also increased logarithmically with height above 500 m with a trend of rougher exposures corresponding to larger veering angles. A number of empirical parameters for engineering applications were presented, including the speed adjustment factors, power exponents of speed profiles, and veering angle, etc. The objective of this study aims to provide useful information on boundary layer wind characteristics for wind-resistant design of high-rise structures in coastal areas.

Keywords: tropical cyclone; wind profile; boundary layer; hilly terrain; Doppler radar

1. Introduction

Typhoon, or strong tropical cyclone (TC), is one of the most destructive natural disasters in the world and may cause severe economic losses and great casualties in areas along coasts and several hundred kilometers inland. As the fast development of modern coastal cities as well as the construction of a plenty of large scale structures, such as high-rise buildings, long-span bridges on seashores and offshore platforms, which are quite sensitive to strong winds, there is an urgent need to understand typhoon wind characteristics and improve structural design codes of practice to address the design requirements for the typhoon effects.

Past studies have revealed a general structure for a mature typhoon commonly consisting of a typhoon eye, eye-wall and spiral rainbands radially within the boundary layer, and some typical features that are very much different from the monsoon winds (Shapiro 1983, Weatherford and Gray 1987, Wurman and Winslow 1998, Wang and Wu 2004, Foster 2005). Based on the

*Corresponding author, Professor, E-mail: bcqqli@cityu.edu.hk

observations made over the last several decades, several typhoon models (Holland 1980, Georgiou 1985, Meng *et al.* 1995, Vickery *et al.* 2009a, Kepert 2001) were established, and were applied to weather forecast, wind-resistant designs of important structures, risk and disaster assessment, etc. However, as typhoon is a kind of complex mesoscale storm, and that it is susceptible to lots of uncertain factors such as local land/sea surface temperature and roughness, transportation of interface thermal energy and landfall conditions, the prediction results from these typhoon models may differ with each other (Vickery *et al.* 2009a), and the outputs of some models showed certain levels of discrepancy with actual situations. Hence, it is necessary to conduct more observations of typhoon wind characteristics, especially of the vertical wind profiles.

Traditional measurements on wind profiles usually make use of towers that are equipped with meteorological devices. Such towers may be erected to several hundred meters high and provide records of wind velocity in these limited height ranges (Monim and Hu 2005, Li *et al.* 2009, 2010). With the development of remote sensing techniques in recent years, Doppler radar and sodar profilers are increasingly adopted for higher vertical range measurements (Knupp *et al.* 2005, Tamura *et al.* 1999, 2007). Recently, NOAA (National Oceanic and Atmospheric Administration of the U.S.) has developed another kind of measurement tool - GPS dropsondes, and conducted a series of investigations on TCs in both eye-wall and outer regions over deep oceans (Franklin *et al.* 2002, Powell *et al.* 2003, Schwendike and Kepert 2007, Vickery *et al.* 2009b, Giammanco *et al.* 2012a, 2012b). They found the log-law was generally valid for the mean wind speed profiles below about 300 m, and the roughness length, friction velocity as well as drag coefficient varied with the mean boundary layer (MBL) wind speed.

According to our statistical analysis of the information published by Hong Kong Observatory (HKO), TC storms formed approximately 27 times in the western Pacific Ocean and in the South China Sea each year since 1970. There were about 6 of them moving close or across Hong Kong or the southeast coastal region of mainland China. This makes Hong Kong a favorite location for the investigation of TC wind field.

In the wind-resistant design of high rise buildings, it is essential to determine the design wind speed profile at the building site. However, there are insufficient data available for TC profiles at some coastal areas where TC storms attack frequently. In order to provide useful information on the TC wind characteristics in the boundary layer, this study presents selected results of wind profiles based on the records from both a Doppler radar wind profiler system and a meteorological anemometer at a coastal island weather station in Hong Kong. The wind data used in this study were measured during 16 tropical cyclones during the years of 2006-2010. The effective measurement range of the radar reached up to 1650 m from a level of 200 m above local ground, while the anemometer supplemented wind data near the ground (at 27 m). With the synchronized measurements from both the radar and the anemometer, the vertical distributions of wind speed and wind direction within the whole boundary layer were obtained. Profilers of horizontal mean wind speed and direction were presented and discussed by groups of wind strength and exposure.

2. Observation station and dataset

The observation station is located at Cheung Chau island (CCH, hereafter) - an island with a height of 72 m in the southwest of Hong Kong, as shown in Fig. 1. In the south semi-plane of CCH, the exposure is dominated by open sea and some small islands; while in the north

semi-plane, CCH is surrounded by a number of mountains (several peaks exceed 800m) and the terrain becomes more complicated.

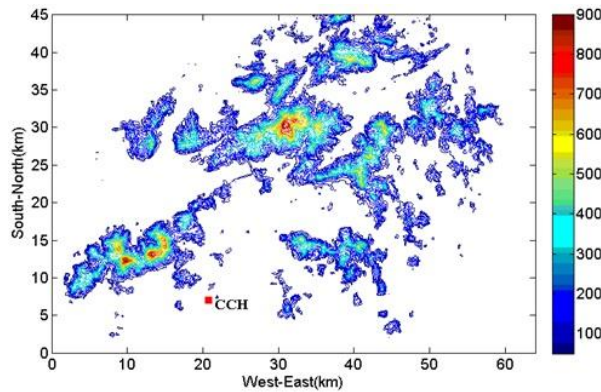


Fig. 1 Location of the CCH station in Hong Kong

The CCH weather station is equipped with a Doppler radar wind profiler (boundary layer type with an operating frequency of 1299 MHz, model: LAP-3000), an anemometer and other meteorological instruments such as thermometer and barometer. The anemometer is installed at a height of 27 m above local ground, or 99 m above mean sea level. It can provide minute-to-minute updated wind information which consists of 1 min mean speed & direction and 3 s peak gust.

The profiler system has a detection resolution of 60 m along height. The observation range extends from 213 m to 1656 m above the ground level. To probe the velocity of atmosphere, the profiler system sends out three beams in every 30 s interval: a vertical beam and two orthogonal oblique beams with an inclination angle of 15° from the zenith. Each beam is capable of measuring at 25 vertical levels equally distributed within 213-1656 m. The system automatically computes the mean horizontal wind speed and direction over a period of 10 minutes. Due to adopting a sliding window technique, the 10 minute mean wind records are updated every 1 to 2 minutes. The profiler system labels each of the level points according to signal noise ratio and consistency: 0 as for credible, 7 as for suspicious and 8 as for inconsistent or missing data.

The remote sensing system is quite sensitive to the atmosphere environment and may be also influenced by the clutter effect (e.g., due to sea waves, aircraft, trees and power-lines reflecting the side lobes emitted from the radar). Consequently, an individual profile commonly contains fewer than 25 credible level records. Thus, to achieve a balance between the quantity and quality of the data for further analysis, this study adopts a criterion that each effective profile should contain at least 20 credible level points for the data quality control. The suspicious level records of these selected profiles are discarded directly.

Profiles from the radar profiler and the anemometer records were then synchronized with each other according to the recording times. The mean wind speed from the anemometer was calculated with an overlapping method following the way adopted in the profiler system. In this study, the mean wind speed and direction were computed in scalar and vector average methods, respectively. Such an operation would avoid an underestimation of wind strength due to vector superposition for speed, and the discontinuity for direction around 0° through arithmetical average.

The final dataset for further study consists of about ten thousand individual profiles from 16 TC storms during the years of 2006-2010. These cyclones affected Hong Kong directly and caused the HKO to raise No. 3 Strong Wind Signals (10 min mean surface speed between 11-17 m/s) up to No. 9 Increasing Gale or Storm Signals (up to 32 m/s). For each cyclone, only the data recorded during the period for the issuance of the Strong Wind Signals were adopted in this paper. Table 1 lists the information of these TCs and the amount of individual profiles obtained from each cyclone.

Table 1 Amount of qualified profiles from 16 TCs (Date: HK local time; Distance: minimum distance from HK to TC center with corresponding direction; Strength: current strength when TC nearest to HK; T.: typhoon; T.S.: tropical storm; S.T.S.: Severe tropical storm; \hat{U} , \hat{u} : maximum mean and gust surface wind speeds in unit of km/h at CCH; WS No.: warning signal No.)

TC name	Date(y/m/d)	Distance(km)	Strength	\hat{U}	\hat{u}	WS No.	Amount
Chanchu	06/05/17	220-ESE	T.	62-NNW	92-N	3	372
Chanthu	10/07/21-22	330-WS	T.	52-ES	68-ESE	3	815
Fanapi	10/09/20-21	150-N	T.S.	49-S	81-WSW	3	1056
Fengshen	08/06/24-25	60-E	S.T.S.	70-WSW	108-WSW	8	816
Goni	09/08/4-5	110-SW	S.T.S.	67-ESE	85-ESE	8	448
Hagupit	08/09/23-24	180-SES	T.	108	153-NE	8	431
Kammuri	08/08/5-6	180-S	S.T.S.	83-ENE	124-NE	8	570
Megi	10/10/21-22	430-ESE	T.	47-NEN	72-NEN	3	347
Molave	09/07/18-19	40-NEN	T.	63-W	103-WSW	9	475
Mujigae	09/09/10-11	330-S	T.S.	51-E	79-ESE	3	348
Nangka	09/06/26-27	60-NE	T.D.	31-E	58-E	3	626
Neoguri	08/04/18-19	150-WNW	T.S.	76-ESE	117-ESE	3	370
Nuri	08/08/21-23	0	S.T.S.	88-SSW	126-SSW	9	746
Pabuk	07/08/9-11	30-W	T.S.	67-NNE	112-N	8	1357
Soudelor	09/07/11	240-S	T.S.	43-ESE	79-SE	3	201
T.D. 2	06/09/13	180-SW	T.D.	47-ESE	85-ESE	3	368

3. Log-law and power-law

Under neutral stability conditions which usually correspond to strong wind cases, the vertical profile of mean horizontal wind speed within the boundary layer is controlled by surface roughness, depicted by the logarithmic law (Paulson 1970)

$$U(z) = (U_*/k) \ln(z/z_0) \quad (1)$$

where U is the mean speed at height z , U_* the friction velocity, z_0 the surface roughness length scale, and $k \approx 0.4$ the von Karman constant. Geometrically, in a semi-log coordinate system, the term in the former parenthesis is the slope of the profile curve, and the roughness length is the intercept. The friction velocity is closely related to the shear stress as

$$\tau = \rho U_*^2 = \rho C_d U_{10}^2 \quad (2)$$

in which ρ is the air density, C_d and U_{10} are the drag coefficient and the mean speed at 10 m surface height, respectively. The log-law works well for smooth surface such as over ocean. But,

when it comes to rougher terrain conditions, the original equation should be corrected by an additional parameter, namely, the zero-plane displacement d , since "the mean flow does not necessarily penetrate downward to the very bottom of the roughness layer" (William and Wilfried 1986, Li *et al.* 2010). However, since this study is based on observations at a coastal island, the log-law model of Eq. (1) is still adopted.

Power law is another widely used equation for the estimation of wind profile (Davenport 1965)

$$U(z) = U_{ref}(z/z_{ref})^\alpha \tag{3}$$

where U_{ref} represents the speed at a reference height z_{ref} , α is the power exponent which reflects the ground roughness condition. Although the power law was proposed empirically, it has been proven to be a reasonable description for a number of terrain conditions. Thus, it has been adopted by some wind load codes in a number of countries, such as in GB 50009-2012 (China). This law is also adopted in this study.

4. Analysis method

Previous studies have shown that single profile from either core area of TC eye-wall or outer peripheral regions could hardly reflect general regularities, due to the common existence of convection, gust, turbulence and other uncertain factors (Franklin 2002). But the statistical information from ensemble profile groups, comprised by a large number of individual profiles, is much more consistent and credible. Therefore, ensemble profile has been widely adopted in the investigations of wind profiles (Franklin 2002, Powell *et al.* 2003, Tamura *et al.* 2007).

Table 2 Amount of profiles by groups of reference speed and reference direction

TC name	$\theta 1$							$\theta 2$					
	V1	V2	V3	V4	V5	V6	V7	V1	V2	V3	V4	V5	V6
Chanchu	0	0	0	0	5	0	0	2	0	0	152	207	6
Chanthu	0	233	503	57	0	0	0	0	12	0	0	0	0
Fanapi	61	420	193	45	10	0	0	0	201	126	0	0	0
Fengshen	0	21	9	195	155	48	0	17	236	35	92	8	0
Goni	0	1	300	48	0	0	0	0	2	87	10	0	0
Hagupit	0	7	74	41	28	58	4	0	22	171	16	10	0
Kammuri	0	0	2	98	64	1	0	0	172	167	42	21	3
Megi	0	0	0	0	0	0	0	0	19	326	2	0	0
Molave	0	84	63	73	50	11	0	17	144	2	10	18	3
Mujigae	0	2	18	3	0	0	0	0	127	179	19	0	0
Nangka	1	223	156	3	0	0	0	13	179	49	2	0	0
Neoguri	0	4	43	141	104	14	0	0	0	48	16	0	0
Nuri	65	28	79	94	45	104	66	49	57	32	30	51	46
Pabuk	13	512	479	148	43	22	0	0	57	53	17	13	0
Soudelor	0	3	30	0	0	0	0	0	30	138	0	0	0
T.D. 2	76	58	52	14	0	0	0	0	1	148	19	0	0
Total	216	1596	2001	960	504	258	70	98	1259	1561	427	328	58

In this paper, the datasets are classified by categories of reference wind speed and reference wind direction. A reference wind speed is defined as the mean boundary layer (MBL) speed of all the level points below 500 m. The reference speed is divided into 7 categories with a step of 5 m/s, i.e., 0-5, 5-10, 10-15, 15-20, 20-25, 25-30, and 30-35 m/s, denoted as V_i , $i=1,2,3,\dots,7$, respectively. The reference wind direction is classified into two categories according to upwind terrain conditions: 90° - 180° - 270° and 90° - 0° - 270° , denoted as $\theta 1$ and $\theta 2$, respectively. Here, the direction is defined positive from the north.

The MBL wind rather than the one at a single level point is adopted as reference herein to avoid a “conditional ensemble average” phenomenon due to the inconsistent correlations at the reference height and at those others (Tamura *et al.* 2007). This is because the MBL speed contains all the boundary layer measurements and is able to reflect an integrated condition (Powell *et al.* 2003).

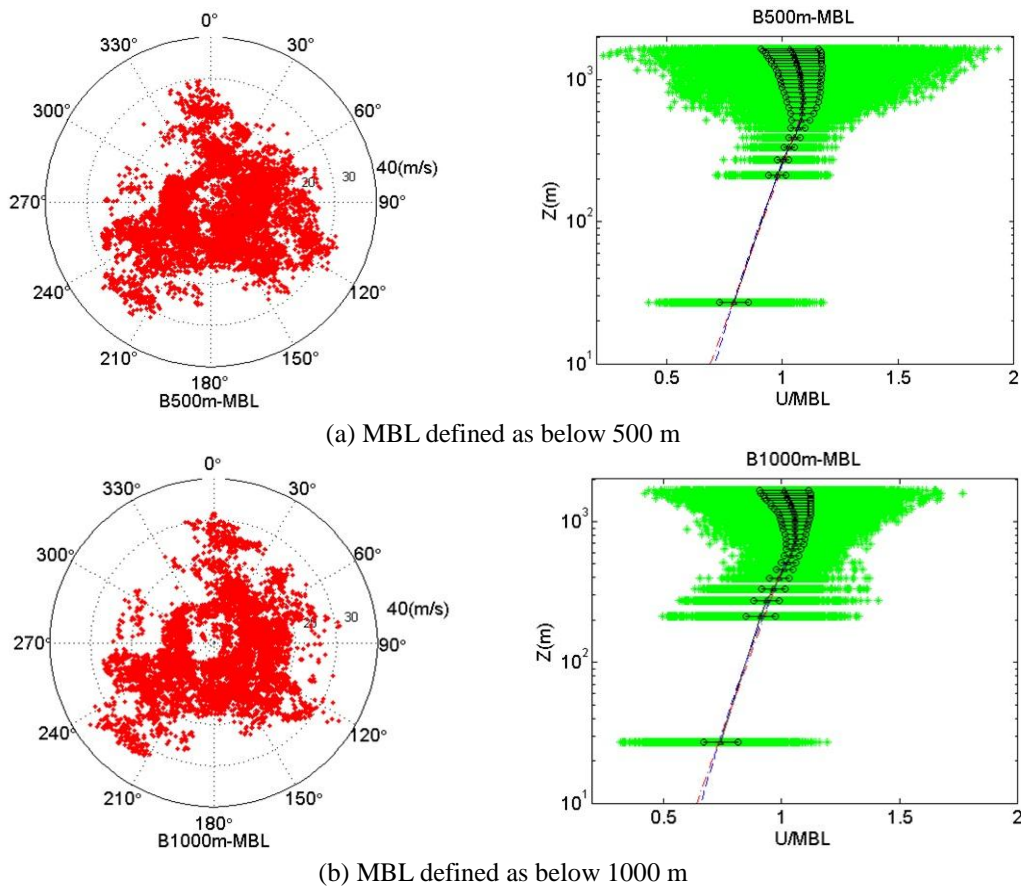


Fig. 2 Polar plots of MBL velocity and normalized profiles in $\theta 1$ sector based on individual profiles with a MBL speed larger than 15 m/s (stars: level records, triangles: ensemble mean speed, horizontal line with circles: standard deviation of ensemble speed, dash dot line: log-law fitting, dash line: power-law fitting, fitting is based on the lowest 7 levels)

But definition of the MBL varied among previous studies owing to the different selection of

boundary layer depths. It is found in this study that different MBL definitions may lead to non-ignorable divergence of obtained results. We have considered 6 options for the MBL definition, namely, below 400 m, 500 m, 700 m, 1000 m, 1300 m and 1650 m, respectively. It is found that: (1) a wider MBL range commonly corresponds to a larger reference speed and reference direction. (2) In general, the wider the MBL range is, the more divergent the lower altitude part of the ensemble profile is, and the more convergent the upper ensemble profile part is.

Fig. 2 presents the polar plots of the reference speed and the normalized ensemble profiles for the cases with MBL defined as below 500 m and 1000 m, respectively. As can be reflected, the MBL defined as below 500 m provides a more compact trend in the height range below this altitude and also shows good consistency with the case of other options at the upper altitude part. Therefore, the MBL below 500 m is adopted. Table 2 lists the distribution information of those selected profiles by groups of reference speed and reference direction which are defined in the way introduced above.

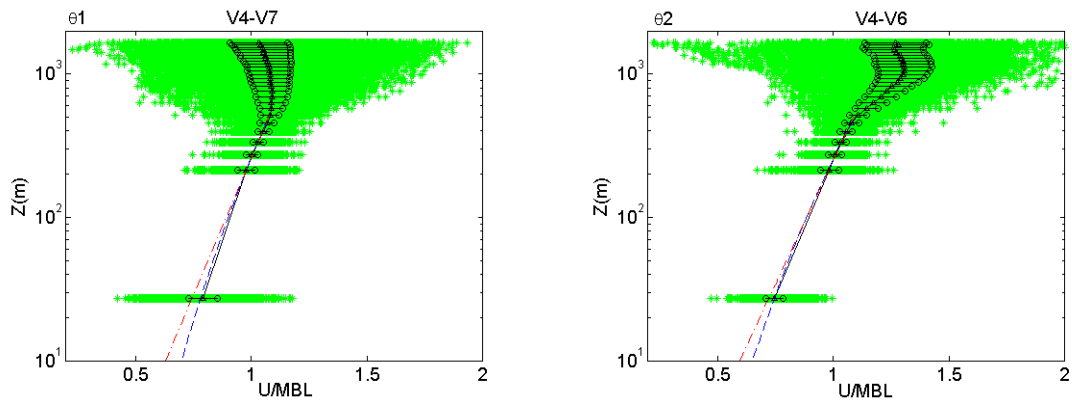


Fig. 3 Normalized ensemble profiles for $\theta 1$ & $\theta 2$ sectors

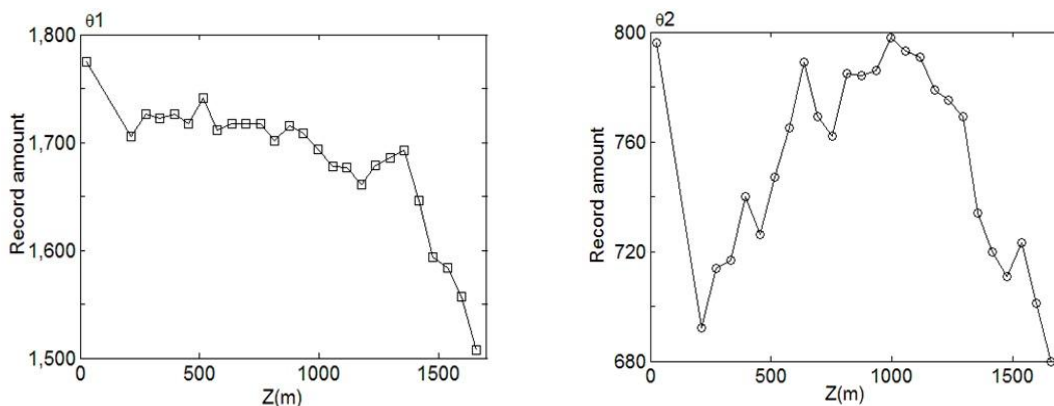


Fig. 4 Distribution of credible level amount for the normalized ensemble profiles

5. Data results

5.1 Normalized ensemble speed profiles

Fig. 3 shows the ensemble profiles normalized by the MBL speeds of those individual profiles with the reference speed larger than 15 m/s. The distribution of credible level amount is depicted in Fig. 4. The ensemble mean speed profiles were fitted by the log-law and the power-law, using the least square method, on the basis of the lowest 6 level points (213-513 m) from the radar system. As can be seen, the regression lines made good fits for the lower ranges below 500 m, and their extended lines nearly passed through the surface (27 m) level point where the wind data were recorded by the anemometer. The differences between the fitted values and the observations at the surface level should be attributed to the hilly speed-up effect on in-situ measurements from the anemometer, although this surface observation device has been installed at a relatively higher level of 27 m above local ground to diminish this topographic influence. Despite these differences, the data measured from the remote sensing system and those from the anemometer actually agree well with each other. The profiles demonstrate a consistent logarithmic or exponent increase with altitude from the surface level to the height of 500 m.

The ensemble mean normalized profiles with different upstream terrains, shown in Fig. 3, have similar trends in the height range below 500 m. The ratios of the 10 min mean speed at 10 m height, the MBL speed and that at 500 m height level are 0.67:1:1.08 and 0.65:1:1.1 for $\theta 1$ and $\theta 2$ sectors, respectively. For both of the two cases, the ensemble mean speeds at the height of 260 m equal to their MBL values. Compared with the result obtained over deep oceans, for which the ratio between the wind speed at 10 m height and the MBL speed was 0.78 (Powell *et al.* 2003), the wind speed profiles measured in this study decreased a bit faster. In the upper levels, single profile has significant discrepancy from the ensemble mean one for both categories. Besides the factor of convective scale features of TC structure as described by Powell *et al.* (2003), the decreasing amount of credible levels at the upper heights, as shown in Fig. 4, and the selection of MBL range may be other reasons for the discrepancy.

The major difference between the profiles of these two categories lied in the additional speed shear in the height range between 500 m and 1000 m for the $\theta 2$ sector which resulted in two yielding points at around 500 m and 1000 m. For $\theta 1$, there was only one yielding point located at around 500 m. Under this altitude, the mean wind speed was dominated by underlying surface roughness and increased logarithmically with height. Above this altitude, due to the weakening deficit pressure between the TC center and peripheral atmosphere (Haurwitz 1935), wind speeds began to level off and then decreased. But for $\theta 2$, while the upper part of the profile above 1000 m was affected by the weakening deficit pressure and varied in a similar way to that in $\theta 1$, the lower part was influenced by both hilly and open sea terrain features. Wind flows blowing from the north semi-plane were obstructed by 400-900 m high mountains (Fig. 1). Consequently, the speed was weakened due to this shielding effect. Such hilly influences persisted until certain distances away from these obstacles, depending on wind strength, mountain sizes and ground roughness conditions (Cao and Tamura 2005, 2007). Inside the intermediate zone for the wind speed recovery, winds at higher altitudes were affected by the hilly upwind terrain, while those at lower altitudes were dominated by underlying seawater terrain.

5.2 Speed profiles by group of reference speed

Fig. 5 depicts the mean speed profiles by group of reference speeds in both $\theta 1$ and $\theta 2$ sectors. Under strong wind conditions (then, thermal effect can be commonly regarded very weak), profiles in both sectors followed the log-law well below 500 m. Table 3 lists the fitting results of these profiles by using both the log-law and power-law based on the lowest 7 level records. Despite the differences of the upwind terrains, the values of the two sectors show much consistency with each other. The obtained exponent of the power-law agrees well with that recommended (0.12) by the current design code of China (GB 50009-2012) for coastal areas. The friction velocity is also compatible with the result from GPS-dropsonde measurements over deep oceans (Powell *et al.* 2003), although the roughness length and drag coefficient obtained in this study are relatively larger due to different observation conditions. There are relatively larger differences between the values of the $\theta 1V6$, $\theta 2V2$ and $\theta 2V3$ groups with those of other groups, which may be, to a large extent, due to lack of lower level records between 27 m and 213 m as well as fitting errors.

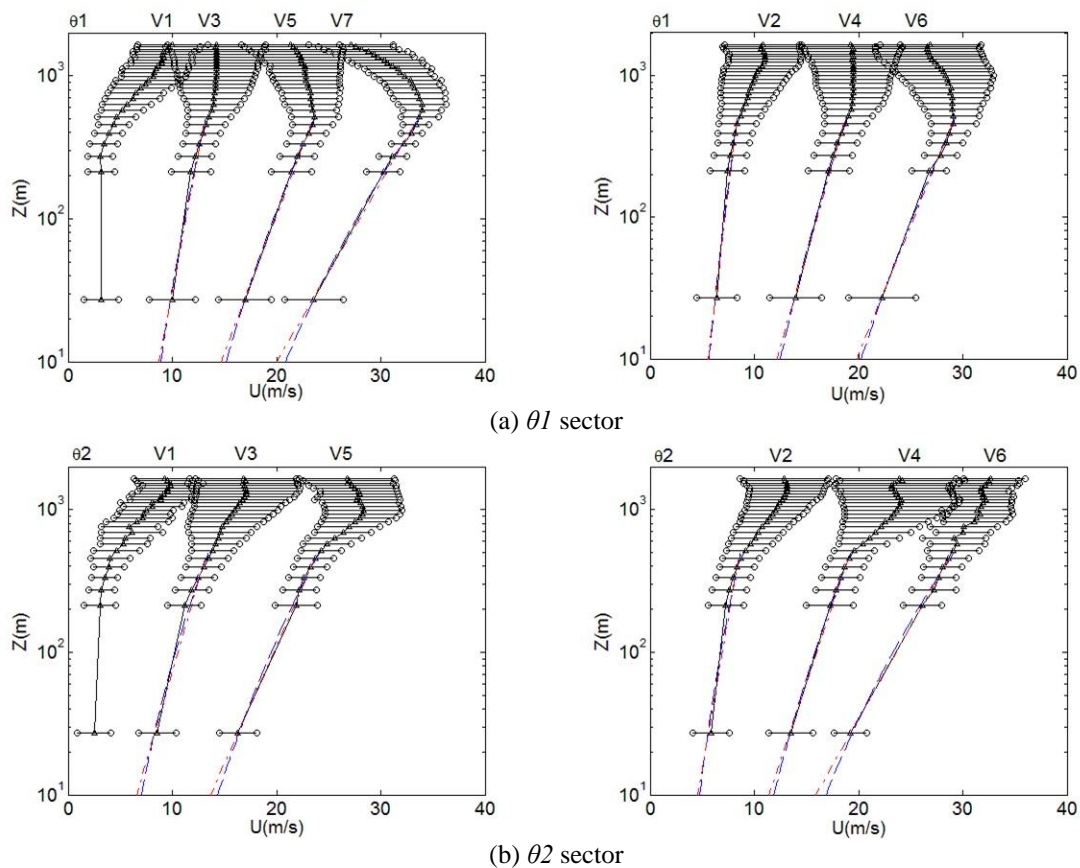


Fig. 5 Ensemble mean speed profiles by group of reference speed

The variations of the estimated mean wind speed and friction velocity at 10 m height as well as the power exponent, with respect to the ensemble-mean reference speed, were fitted by linear models. The roughness length was fitted by a power-law. This study did not make an attempt to fit

the measured data for the determination of the drag coefficient, since it can be directly deduced from Eq. (2) with other given parameters. The obtained results are shown in Fig. 6 and Eqs. (4)-(7). These parameters basically demonstrate a trend of increasing with the reference speed. Under similar MBL speed conditions, except that U_{10} in $\theta 2$ is somewhat larger than that in $\theta 1$, all other parameters in $\theta 1$ are a bit smaller than those in $\theta 2$.

Table 3 Fitting results of mean speed profiles by group of reference speed using the log-law and power-law

	$\theta 1$						$\theta 2$				
	V2	V3	V4	V5	V6	V7	V2	V3	V4	V5	V6
U_{MBL}	7.82	12.3	17.5	21.9	27.5	31.0	7.84	12.1	17.8	22.0	26.6
α	.100	.102	.105	.114	.094	.123	.154	.167	.124	.132	.140
U_{10}	5.66	8.87	12.5	15.2	20.3	20.8	4.76	7.01	11.9	14.4	16.9
U_*	.284	.455	.674	.909	.961	1.38	.412	.688	.795	1.05	1.34
z_0	.0040	.0048	.0073	.016	.0026	.031	.119	.218	.032	.055	.087
C_d	.0025	.0026	.0029	.0036	.0022	.044	.0075	.0096	.0045	.0054	.0063

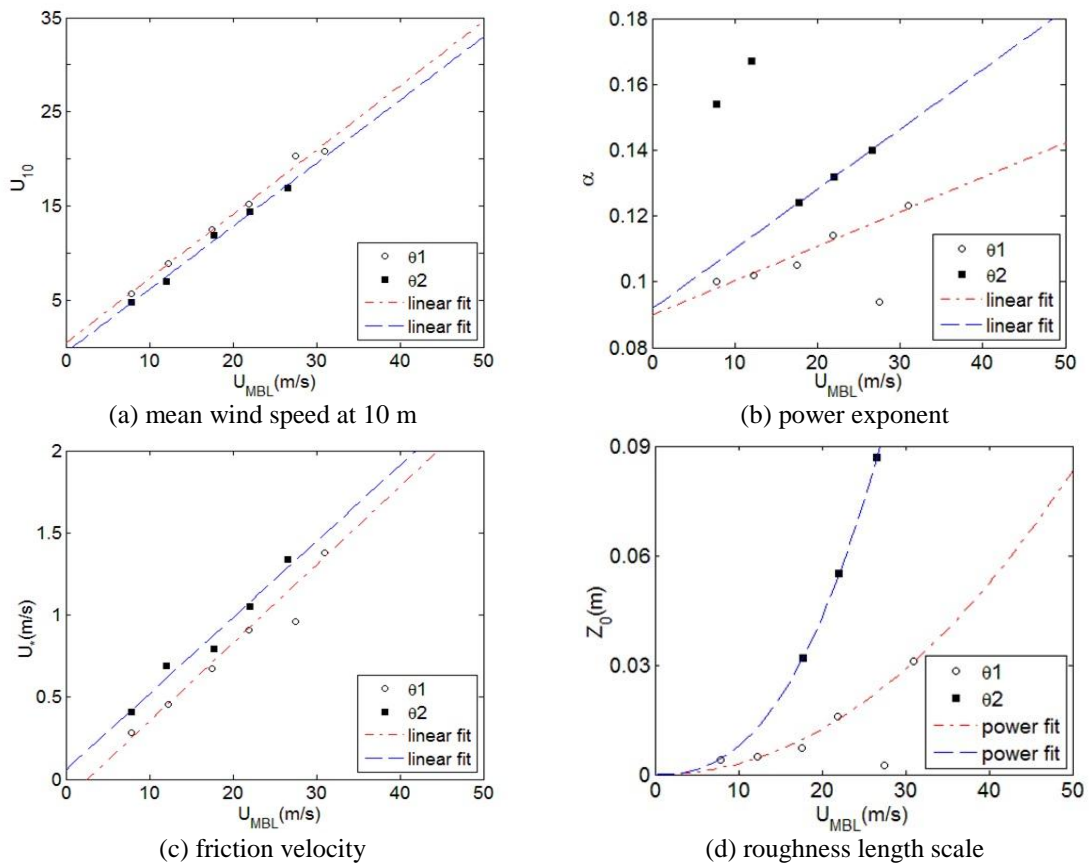


Fig. 6 Correlations between calculated log-law and power-law parameters and MBL speed

$$U_{10}^{\theta 1} = 0.68U_{MBL}, \quad U_{10}^{\theta 2} = 0.67U_{MBL} \quad (4)$$

$$\alpha^{\theta 1} = 0.090 + 0.0010U_{MBL}, \quad \alpha^{\theta 2} = 0.092 + 0.0018U_{MBL} \quad (5)$$

$$U_*^{\theta 1} = -0.123 + 0.0476U_{MBL}, \quad U_*^{\theta 2} = 0.057 + 0.0464U_{MBL} \quad (6)$$

$$z_0^{\theta 2} = 2.49 \times 10^{-5} (U_{MBL})^{2.075}, \quad z_0^{\theta 2} = 2.63 \times 10^{-5} (U_{MBL})^{2.471} \quad (7)$$

5.3 Profiles of wind direction

5.3.1 Ensemble direction

Fig. 7 shows the ensemble mean profiles of horizontal wind direction by groups of reference speed and direction. To get more detailed information, the reference direction groups are refined into 6 categories of 0-60°, 60-120°, 120-180°, 180-240°, 240-300° and 300°-360°. Table 4 lists the distribution of individual profile amount among these groups. In low speed cases, owing to the fact that there were more times to respond sufficiently for thermal effects (Tamura *et al.* 2007), these weak winds demonstrated significant divergence along height. Thus, profiles in the VI group were excluded for further analysis. Basically, despite the difference of wind strength, the direction profiles in the same reference direction group show much a consistent trend of increasing with height. This is attributed to the Ekman Spiral Effect due to the Earth's rotation (Price *et al.* 1986, Richman *et al.* 1987). However, profiles in different reference direction groups, corresponding to varied upwind terrains, differ with each other visibly.

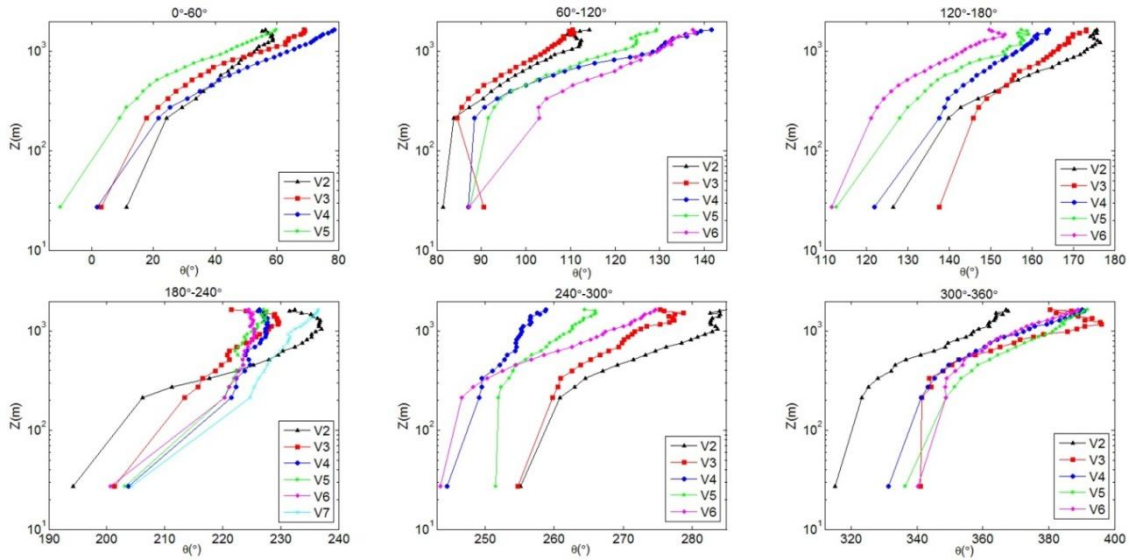


Fig. 7 Directional ensemble profiles of horizontal mean wind direction

Table 4 Distribution of individual profile amount among different reference speed and direction groups

Sectors	V1	V2	V3	V4	V5	V6	V7	Total
0-60°	48	443	774	236	104	5	0	1562
60-120°	41	743	967	244	116	41	3	2114
120-180°	106	474	732	249	88	38	1	1582
180-240°	80	338	527	329	157	136	66	1553
240-300°	25	616	446	244	203	54	0	1563
300-360°	14	241	126	85	164	42	0	658

5.3.2 Veering angle

The ensemble profiles in the same reference direction group are used to generate another kind of profiles, composed of the veering angles at different height levels relative to the surface wind at 27 m. The results are shown in Fig. 8(a). It is very interesting to note that profiles in the pair of diagonally distributed azimuthal groups (e.g., 0-60° & 180-240°) are more closely coupled with each other in the lower boundary layer. This may suggest that winds blowing in these opposite azimuthal sectors were affected by similar terrain and/or topographic features. However, in the upper boundary layer, these coupled profile pairs are decoupled gradually. They were mainly affected by upwind topographic features. The more mountainous the upwind topography is, the larger the veering angle becomes.

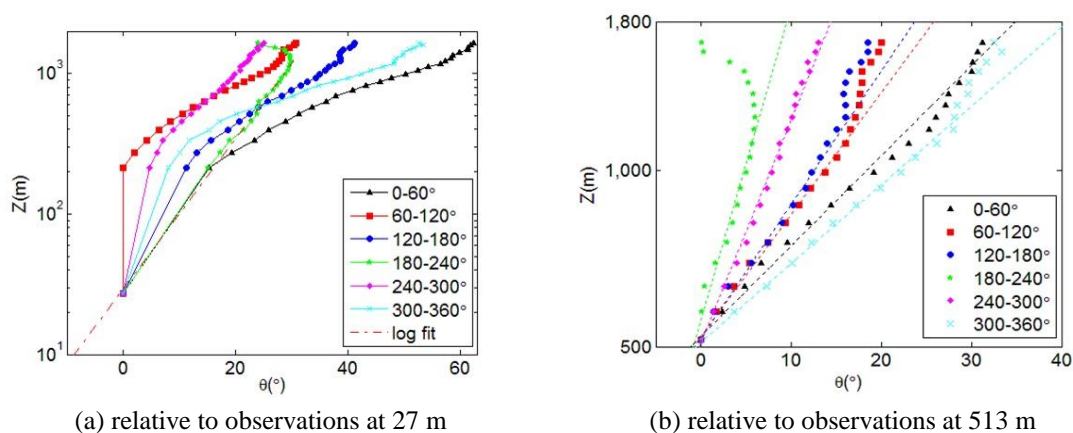


Fig. 8 Profiles of veering direction

The profile in the group of 180-240° is distinguished from others by its uniformly logarithmical increase with altitudes as far as up to about 1200 m where the veering angle levels off and then begins to decrease. This group corresponds to an open sea upwind terrain. Thus, the mean wind direction experiences a consistent change in both lower and upper altitudes. Meanwhile, from Tables 1 and 4, this group also contains the strongest winds during Typhoon Nuri. Fig. 9 depicts the track and the velocity variations during Typhoon Nuri passing over Hong Kong, which shows that Nuri entered and left the measurement station with north and southwest wind directions, respectively. Thus, the strongest winds in this group were measured in Nuri's inner areas where the

free atmosphere height defined by the level with zero inflow-angle is relatively lower than those of outer regions (Giammanco *et al.* 2012b). So in the sector of 180-240°, the veering angle profile got a maximum value at 1200 m. At a given height below this free atmospheric level, the veering angle can be calculated as

$$\gamma = 7.94 \ln(z/27), 27 \leq z \leq 1200 \quad (8)$$

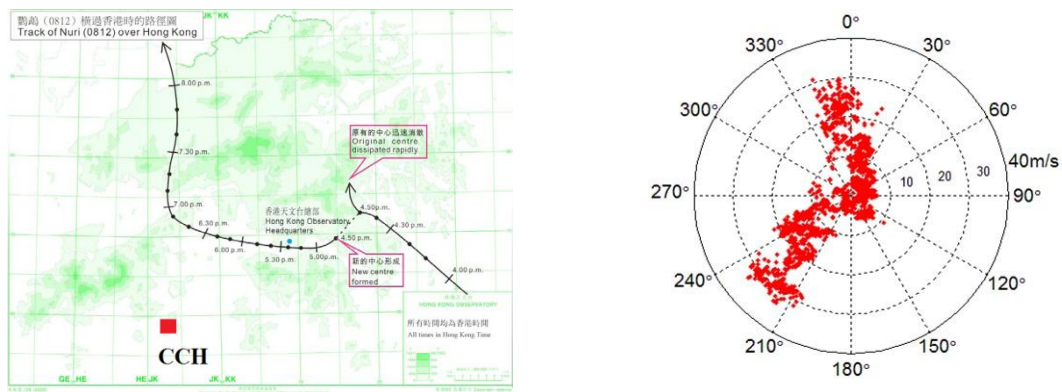


Fig. 9 Center track of Typhoon Nuri and the polar distribution of measured surface mean speed

Fig. 9 illustrates that the 300-360° sector also contains profiles measured in the inner area of Typhoon Nuri. But compared to the case in the sector of 180-240°, there were no yielding points in the ensemble profiles of rotating angle for these two sectors. This should be attributed to the influence of hilly upwind terrain.

Profiles of veering angle above 500 m are shown in Fig. 8(b). Basically, they increase linearly in the semi-log coordinate. For the 6 sectors, the slopes are 28.1, 20.9, 19, 8.12, 11.4 and 32.3, respectively which reflect the upwind topographic conditions.

The vertical distributions of wind speed and wind direction share some common features such as the same yielding point at 500 m height. This may suggest a close correlation between these two parameters. But, they also differ with each other. A typical example is that, between the height of 500 m and 1200 m, the wind direction changed monotonically with height. By contrast, the distribution of mean wind speed was more complicated due to the weakening of TC central deficit pressure.

6. Conclusions

Based on the 5 years' dataset of tropical cyclones from both Doppler radar wind profiler and an anemometer at a coastal island site, this paper investigated the vertical profiles of mean wind speed and wind direction and discussed the influences of wind strength and upwind terrain on the profiles. The main conclusions are summarized as follows:

- The ensemble mean wind speed profiles follow the log-law and power-law below 500 m for both hilly upwind terrain and open sea upwind terrain. In the upper part, the profiles leveled off

and began to decrease with altitudes due to the weakening deficit pressure between TC center and ambient atmosphere.

- The proportions of the mean wind speeds at 10 m height, the MBL speed and that at 500 m height are 0.67:1:1.08 and 0.65:1:1.1 for $\theta 1$ and $\theta 2$ sectors, respectively.
- The fitting parameters of the log-law and power-law in different reference speed groups increased consistently with the MBL speed. The friction velocity and the power exponent showed a linear increase, while the roughness length depicted an exponential increase. Basically, fitting parameters in $\theta 1$ were a bit smaller than those in $\theta 2$.
- The major difference of mean speed profiles between $\theta 1$ and $\theta 2$ was the additional speed shear between 500-1000 m in the latter sector, which should be attributed to the hilly effect.
- Profiles of the mean horizontal wind direction were also influenced by local terrain setups and upwind topographic features. For a uniform off sea exposure, the wind direction increased logarithmically with height up to 1200 m. The veering angle within this range was 30°.

Acknowledgments

The authors would like to express their gratitude to HKO for the provision of the wind data records and the permission of using the data for this study. The work described in this paper was supported by a grant from the Research Grants Council of Hong Kong Special Administrative Region, China (Project No: CityU 117709) and a research grant from the Research Committee of City University of Hong Kong (Project No. 7002615).

References

- Cao, S.Y. and Tamura, T. (2005), "Experimental study on roughness effects on turbulent boundary layer flow over a two-dimensional steep hill", *J. Wind Eng. Ind. Aerod.*, **94**(1), 1-19.
- Cao, S.Y. and Tamura, T. (2007), "Effects on roughness blocks on atmospheric boundary layer flow over a two-dimensional low hill with/without roughness change", *J. Wind Eng. Ind. Aerod.*, **95**(8), 679-695.
- Davenport, A.G. (1965), "The relationship of wind structure to wind loading", *Proceeding of the Symposium on Wind Effect on Building and Structures*, London.
- Franklin, J.L., Black, M.L. and Valde, K. (2002), "GPS dropwindsonde wind profiles in hurricanes and their operational implications", *Weather Forecast.*, **18**, 32-44.
- Foster, R.C. (2005), "Why rolls are prevalent in the hurricane boundary layer", *J. Atmos. Sci.*, **62**, 2647-2661.
- GB 50009-2012 (2012), *Load code for the design of building structures*, Beijing
- Georgiou, P.N. (1985), *Design wind speeds in tropical cyclone-prone regions*, Ph.D Dissertation, University of Western Ontario, Canada.
- Giammanco, I.M., Schroeder, J.L. and Powell, M.D. (2012), "Observed characteristics of tropical cyclone vertical wind Profiles", *Wind Struct.*, **15**(1), 65-86.
- Giammanco, I.M., Schroeder, J.L. and Powell, M.D. (2013), "GPS dropwindsonde and WSR-88D observations of tropical cyclone vertical wind profiles and their characteristics", *Weather Forecast.*, **28**, 77-99.
- Haurwitz, B. (1935), "The height of tropical cyclones and of the 'eye' of the storm", *Mon. Weather. Rev.*, **73**, 45-49.
- Holland, G.J. (1980), "An analytic model of the wind and pressure profiles in hurricane", *Mon. Weather. Rev.*, **108**, 1212-1218.

- Keper, J. (2001), "The dynamics of boundary layer jets within the tropical cyclone core. Part 1: linear theory", *J. Atmos. Sci.*, **58**, 2469-2484.
- Knupp, K.R., Walters, J. and Biggerstaff, M. (2005), "Doppler profiler and radar observations of boundary layer variability during the landfall of tropical storm Gabrielle", *J. Atmos. Sci.*, **63**, 234-251.
- Li, Q.S., Zhi, L.H. and Hu, F. (2009), "Field monitoring of boundary layer wind characteristics in urban area", *Wind Struct.*, **12**(6), 553-574.
- Li, Q.S., Zhi, L.H. and Hu, F. (2010), "Boundary layer wind structure from observations on a 325 tower", *J. Wind Eng. Ind. Aerod.*, **98**(12), 818-832.
- Meng, Y., Matsui, M. and Hibi, K. (1995), "An analytical model for simulation of the wind field in a typhoon boundary layer", *J. Wind Eng. Ind. Aerod.*, **56**(2-3), 291-310.
- Monim, H.A. and Hu, F. (2005), "Surface roughness around a 325-m meteorological tower and its effect on urban turbulence", *Adv. Atmos. Sci.*, **22**, 595-605.
- Paulson, C.A. (1970), "The mathematical representation of wind speed and temperature profiles in the unstable atmospheric surface layer", *J. Appl. Meteor.*, **9**(6), 857-861.
- Powell, M.D., Vickery, P.J. and Reinhold, T.A. (2003), "Reduced drag coefficient for high wind speeds in tropical cyclones", *Nature*, **422**, 279-283.
- Price, J.F., Weller R.A. and Pinkel, R. (1986), "Diurnal cycling: observations and models of the upper ocean response to diurnal heating, cooling and wind mixing", *J. Geophys. Res.*, **91**(7), 8411-8427.
- Richman, J.G., de Szoeke, R.A. and Davis, R.E. (1987), "Measurements of near-surface shear in the ocean", *J. Geophys. Res.*, **92**(3), 2851-2858.
- Schwendike, J. and Keper J. D. (2007), "The boundary layer winds in hurricanes Danielle (1998) and Isabel (2003)", *Mon. Weather. Rev.*, **136**, 3168-3192.
- Shapiro, L.J. (1983), "The asymmetric boundary layer flow under a translating hurricane", *J. Atmos. Sci.*, **40**, 1984-1998.
- Tamura, Y., Suda, K., Sasaki, A., Iwatani, Y., Fujii, K., Hibi, K. and Ishibashi, R. (1999), "Wind speed profiles measured over ground using Doppler sodars", *J. Wind Eng. Ind. Aerod.*, **83**(1-3), 83-93.
- Tamura, Y., Iwatani, Y., Hibi, K., Suda, K., Nakamura, O., Maruyama, T. and Ishibashi, R. (2007), "Profiles of mean wind speeds and vertical turbulence intensities measured at seashore and two inland sites using Doppler sodars", *J. Wind Eng. Ind. Aerod.*, **95**(6), 411-427.
- Wang, Y. and Wu, C.C. (2004), "Current understanding of tropical cyclone structure and intensity changes-a review", *Meteor. Atmos. Phys.*, **87**, 257-278.
- Weatherford, C.L. and Gray, W.M. (1987), "Typhoon structure as revealed by aircraft reconnaissance. Part 1: data analysis and climatology", *Mon. Weather. Rev.*, **116**, 1032-1043.
- William, P.K. and Wilfried, B. (1986), "Wind profile constants in a neutral atmospheric boundary layer over complex terrain", *Bound.-Lay. Meteor.*, **34**(1-2), 35-54.
- Wurman, J. and Winslow J., 1998. "Intense sub-kilometer-scale boundary layer rolls observed in Hurricane Fran", *Science*, **280**(5363), 555-557.
- Vickery, P.J., Masters, F.J., Powell, M.D. and Wadhera, D. (2009a), "Hurricane hazard modeling: the past, present, and future", *J. Wind Eng. Ind. Aerod.*, **97**(7-8), 392-405.
- Vickery, P.J., Powell, M.D. and Chen, Y.Z. (2009b), "A hurricane boundary layer and wind field model for use in engineering applications", *J. Appl. Meteorol. Clim.*, **48**(2), 381-405.